Fuel 334 (2023) 126800

Contents lists available at ScienceDirect

Fuel

journal homepage: www.elsevier.com/locate/fuel

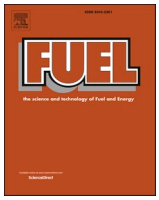

Full Length Article

An effective stress-dependent dual-fractal permeability model for coal considering multiple flow mechanisms

Jianwei Tian [a,*], Jishan Liu [a], Derek Elsworth [b], Yee-Kwong Leong [a], Wai Li [a]

[a] School of Engineering, The University of Western Australia, 35 Stirling Highway, WA 6009, Australia
[b] Department of Energy and Mineral Engineering, G3 Center and Energy Institute, The Pennsylvania State University, University Park, PA 16802, USA

ARTICLE INFO

Keywords:
Coalbed methane
Fractal permeability
Gas sorption
Multiphysics coupling

ABSTRACT

Coal permeability is significantly affected by the multi-scale pore-fracture size distribution. More importantly, the pore-fracture size is changed by the effective stress, swelling/shrinkage under the influence of gas sorption, and different flow mechanisms. In conventional dual-porosity models, these effects are normally studied separately and the impacts of heterogeneous structure on permeability are neglected. In this study, a dual-fractal permeability model was proposed to quantitatively investigate the impacts of coal internal structure on the permeability. In the improved permeability model, the fractal dimension and the pore-fracture size of the coal are linked with porosity, which are dependent on the evolution of effective stress and matrix shrinkage. Besides, multiple flow mechanisms were also incorporated into the model. The proposed model was verified with field data and achieved a good agreement. The sensitivity studies and model results indicate that: (1) pore/fracture size distributions affect the contribution ratios of versatile flow regimes and to total gas flux and the total permeability; (2) fractal dimensions of matrix and fracture systems increase with the decline of pore pressure; (3) increment of matrix permeability is jointly decided by the transition of flow regime and effective stress, while the fracture permeability is dominated by effective stress.

1. Introduction

With the depletion of conventional natural gas, there is an increasing demand for the exploration and exploitation of unconventional natural gas. Typically, coal seam gas (CSG) is a vital substitute that can relieve the energy supply shortage, especially for China, which has deposits ofc1.25 $\times$ $10^{13}m^3$ [1]. Coal permeability is the dominant factor controlling CSG recovery efficiency. Therefore, it is important to have a comprehensive understanding of the influential factors of permeability. To this end, a multitude of investigations has been conducted to reveal the impacts of stress [2–4], gas sorption-induced coal swelling [5–8] and anisotropy [9–11] on permeability evolution. However, the majority of models are based on continuum media, and the impacts of the heterogeneous structure of coal on permeability are neglected.

Coal structure exhibits multi-scale heterogeneity, and the pore size in matrix spans from micrometre to nanometre scales, which affects gas transport and storage capability substantially [12,13]. The heterogeneous pore structure of coal is characterised by the multiscale pore size distribution (PSD), connectivity and the tortuous gas flow path [14]. For both gas recovery and CO2 sequestration, gas transport mechanisms in coal are governed by pore diameter as well as pore pressure. The Knudsen number (Kn), defined as the ratio between the molecular free path and characteristic length, is extensively applied to characterise flow regimes. The gas flow regimes include viscous flow ($Kn < 0.001$), slip flow ($0.001 < Kn < 0.1$), transitional flow ($0.1 < Kn < 10$) and free molecular flow ($Kn > 10$). According to the definition of the Knudsen number, pore size distribution determines the flow regimes in micropores when pore pressure remains constant. Therefore, the pore structure of coal has a significant impact on the apparent permeability of the coal matrix. Different distribution functions have been employed to study the effect of PSD on apparent permeability, demonstrating that permeability is highly sensitive to the variation of the distribution function [15,16]. When the proportion of micropores is larger, the specific surface is also larger, providing much more adsorption space for coal seam gas [15]. The original gas in place (OGIP) and corresponding sorption-induced swelling can be affected significantly as well. For coal seams at different depths, coal swells or contracts greatly depend on PSD [17]. In addition to porosity, the tortuosity of pore structure is an essential parameter for permeability prediction, which reflects the ratio between the actual flow length and the characteristic length of the coal

* Corresponding author.
E-mail address: jianwei.tian@research.uwa.edu.au (J. Tian).

https://doi.org/10.1016/j.fuel.2022.126800
Received 18 August 2022; Received in revised form 5 October 2022; Accepted 13 November 2022

sample. According to the Kozeny-Carman model, there is a negative correlation between permeability and tortuosity [18]. A theoretical investigation indicates that large tortuosity can increase the resistance of gas transport [19].

In recent years, the fractal approach has been widely utilised to investigate the multi-scale distribution of pore size. Research results indicate that the distribution of pore sizes exhibits scale-affine fractal characteristics for coal samples, which necessitate the investigation of multi-scale effects on gas transport capacity [20–22]. X-ray computed tomography (CT) and the mercury intrusion technique have been extensively applied to reveal the microscopic structure based on the digital morphology of coal [23–25]. Therefore, permeability models based on fractal theory have been proposed to incorporate the impacts of PSD and tortuosity. Yu et al. [26] proposed a permeability model based on fractal theory for porous media, which incorporates the basic pore structure parameters. Based on that, the fractal permeability model has been extended to coal and shale [27,28]. However, these studies on fractal theory did not consider the effects of effective stress and gas adsorption on gas transport, which dominate the gas recovery and gas injection processes for ultra-low permeability reservoirs. Currently, most studies concerning fractal permeability are based on the static fractal dimension, which is not consistent with practical situations. Our previous study [29] used the fractal approach to couple gas flow and coal deformation, but the evolution of the pore-fracture size when the effective stress changes was not accommodated in the coupling-based simulation. According to the results of [30,31], the pore diameter in the fractal permeability would decrease with the increase of effective stress. Hence, it is highly essential to incorporate the evolution of pore-fracture size change in the fractal-based permeability model. As the fractal dimension represents the heterogeneity of the reservoir, it can vary when gas pressure decreases and the initial equilibrium fails [32]. Effective stress and sorption-induced swelling stress can contribute significantly to pore contraction or enlargement, thereby altering reservoir permeability.

As reviewed above, multitudes of permeability models have been proposed to incorporate gas sorption-induced coal deformation and gas flow in coal seam gas extraction to reveal the dominant mechanisms controlling permeability evolution [33–35]. However, these studies are based on the assumption that coal structure is homogeneous and the scale effect have been disregarded. Consequentially, few studies consider the effects of the intrinsic structural heterogeneities of coal on permeability and gas migration. Despite the recent applications of fractal theory on coal structure characterisation through experimental approaches, the geo-mechanics and gas adsorption are not accommodated. Therefore, this study proposes an effective stress-dependent fractal permeability model to fully couple the coal deformation, gas flow and gas desorption. The major assets of this model include (1) fine characterisation of matrix-fracture heterogeneities by a dual-fractal approach; (2) integration of the fractally-distributed micro-structures into the multiphysics coupling model. Based on this model, the impacts of structural heterogeneity on permeability evolution are quantitatively investigated. Field data are selected to verify the feasibility and robustness of the model. Finally, the impacts of pore-fracture size and fractal parameters on intrinsic permeability and permeability evolution are investigated. Based on that, the contributions of various mechanisms to permeability enhancement, including the flow regime, effective stress and matrix shrinkage, are illustrated and compared.

2. Model formulation

In this section, a dual-porosity model is formulated to simulate gas transport in heterogeneous coal. Coal matrix heterogeneity is characterized by pore size distribution (PSD) and pore tortuosity. In the continuum model, coal deformation and gas flow are coupled by a fractal-based permeability model and mapped into the same domain with the overlapping approach for the subsequent simulation, as illustrated in Fig. 1. The simulation of this study is based on a single porosity model. The basic assumptions are as follows: (a) coal is an anisotropic and elastic continuum; (b) strains are much smaller than the length scale; (c) gas contained within the pores is ideal, and its viscosity is constant under isothermal conditions; (d) conditions are isothermal; (e) coal is saturated by gas; (f) PSD follows fractal scaling laws in the coal deformation process.

2.1. Governing equations for coal deformation

The relationship between strain and displacement is given by

$$\varepsilon_{ij} = \frac{1}{2}\left(u_{i,j} + u_{j,i}\right) \tag{1}$$

where ε_{ij} is the component of the total strain tensor, u_i is the component of the displacement, the force equilibrium equation can is defined as:

$$\sigma_{ij,j} + f_i = 0 \tag{2}$$

where σ_{ij} denotes the component of the total stress tensor, f_i denotes the component of the body force. The constitutive relation of effective stress is defined as [37]

$$\sigma_{ij} = \left(K - \frac{2G}{3}\right)\varepsilon_{kk}\delta_{ij} + 2G\varepsilon_{ij} - \beta p_f \delta_{ij} - \alpha p_m \delta_{ij} - K\varepsilon_s \delta_{ij} \tag{3}$$

where G is shear modulus, K is the bulk modulus,$K = E/3(1-2\nu)$, ν is Poisson's ratio of coal matrix, α and β are the Biot coefficient,$\alpha = 1 - K/K_s$, $\beta = 1 - K/K_f K_s$ is the bulk modulus of coal grains,p is pore pressure, δ_{ij} is Kronecker delta, and ε_s is sorption-induced strain. According to the mechanical equilibrium equation of the solid medium under effective stress, the equation governing coal deformation is formulated as [37]:

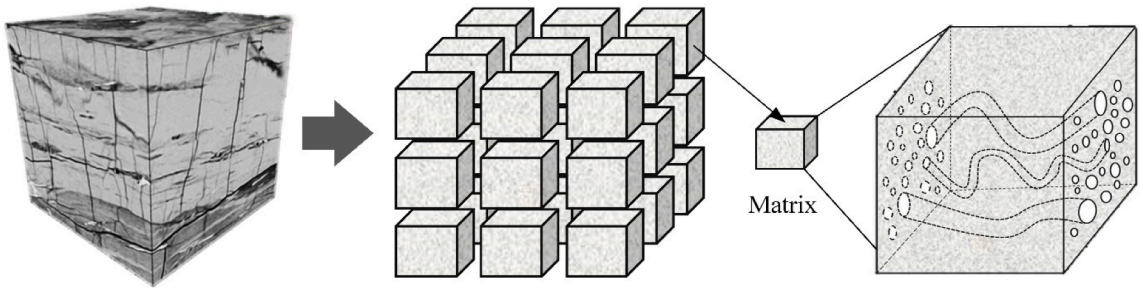

Fig. 1. Fracture-matrix structure of coal: (a) CT image of the matrix-fracture structure (CT image from [36]; (b) the fracture system; (c) the multiscale pores in coal matrix.

$$Gu_{i,kk} + \frac{G}{1-2\nu}u_{k,ki} - \alpha p_{mi} - \beta p_{fi} - K\varepsilon_{s,i} + f_i = 0 \tag{4}$$

The Langmuir type equation has been widely applied to represent the sorption-induced strain in previous reports and is given by [38,39]:

$$\varepsilon_s = \frac{\varepsilon_L p_m}{p_m + p_L} \tag{5}$$

where ε_L and p_L are Langmuir strain constants, ε_L is the ultimate strain when pressure tends to infinity, and p_L is the pressure when the sorption strain is the half value ofε_L.

2.2. Governing equations for gas flow

The balance equation combined with Darcy's law for gas flow through coal is expressed as:

$$\frac{\partial m}{\partial t} + \nabla\cdot\left(-\rho_g\frac{k}{\mu}\nabla p\right) = Q_s \tag{6}$$

where ρ_g is the gas density in pore space, $\rho_g = M_g p/(RT)$, k is the apparent permeability, and Q_s is the source or sink term. The mass change in REV includes both of the free and adsorbed gas and can be written as:

$$\begin{cases} m_m = \rho_g\phi_m + \rho_{ga}\rho_c\dfrac{V_L p_m}{p_m + p_L} \\ m_f = \rho_g\phi_f \end{cases} \tag{7}$$

Substituting Eq. (7) into (6), the mass balance equation can be rearranged to give:

$$\begin{cases} \left[\phi_m + \rho_{ga}\rho_c\dfrac{V_L p_m}{p_m + p_L}\right]\dfrac{\partial p_m}{\partial t} + p_m\dfrac{\partial \phi_m}{\partial t} + \nabla\cdot\left(-\dfrac{k_m}{\mu}p_m\nabla\cdot p_m\right) = \omega(p_f - p_m) \\ \phi_f\dfrac{\partial p_f}{\partial t} + p_f\dfrac{\partial \phi_f}{\partial t} + \nabla\cdot\left(-\dfrac{k_f}{\mu}p_f\nabla\cdot p_f\right) = -\omega(p_f - p_m) \end{cases} \tag{8}$$

where ω is the transfer coefficient between coal matrix and fractures, which is defined as:

$$\omega = 8\left(1 + \frac{2}{a^2}\right)\frac{k_m}{\mu} \tag{9}$$

where a is the shape factor of coal matrix.

2.3. Dynamic permeability model for coal matrix

When gas flows through the micropores of the coal matrix, the pore throat size is comparable to the molecular free path, the rarefaction effect becomes pronounced and the non-Darcy flow gradually dominates. Knudsen number (Kn) is used to divide the various flow regime based on pore size and pore pressure, as shown in Fig. 2. The relationship between the Knudsen number and the molecular free path is defined as:

$$Kn = \frac{\lambda}{h} \tag{10}$$

where the molecular free path (λ) is given by:

$$\lambda = \frac{K_B T}{\sqrt{2}\pi d_c^2 p} = \frac{\mu}{p}\sqrt{\frac{\pi RT}{2M_g}} \tag{11}$$

where K_B is the Boltzmann constant, T is the temperature and d_c is the capillary tube diameter. According to previous reports [40], when the pore diameter is between 10 nm and 1000 nm, the Knudsen diffusion and slip flow coexist.

In Klinkenberg's [41] pioneering research, he proposed a correction model to modify the intrinsic permeability. Since then, several correction models have been proposed to incorporate the Klinkenberg effect (Slip flow), as summarized in Table 1.

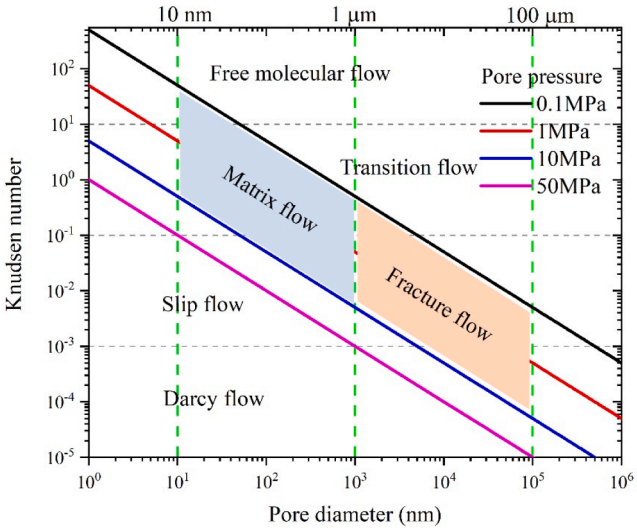

Fig. 2. Evolution of Knudsen number versus pore diameter and pore pressure.

For a single fractal capillary tube, the gas flux incorporated slip effect is expressed as [51,52]:

$$q_{slip} = \frac{\pi h^4}{128\mu}\left(1 + \frac{8\lambda}{h}\right)\frac{\Delta p_m}{L_\tau(h)} \tag{12}$$

When the Kn between 0.1 and 10, the Knudsen diffusion cannot be neglected, the contributed gas flux is expressed as:

$$q_{knudsen} = \frac{h^3}{6p}\sqrt{\frac{2\pi RT}{M_g}}\frac{\Delta p_m}{L_\tau(h)} \tag{13}$$

Therefore, the total gas flux in a single pore can be obtained as:

Table 1
Correction models for Klinkenberg effect.

Model reference	Formula	Parameters
Klinkenberg [41]	$k_a = k_\infty\left(1 + \frac{b}{p}\right)$	$b = \frac{4c\lambda p}{R}$
Ertekin, et al. [42]		$b = \frac{16c\mu}{\omega_{pore}}\sqrt{\frac{2RT}{\pi M}}$
Heid, et al. [43]		$b = \alpha(k_\infty)^\beta$
Florence, et al. [44]		$b = \alpha(k_\infty/\phi)^\beta$
Yao, et al. [45]		$b_k = (D_k\mu)/k_\infty$
Wang, et al. [46]		$b_{CH4} = \frac{\phi_0}{\phi_0 - \varepsilon_s}\frac{\mu_{CF4}}{\mu_{He}}\sqrt{\frac{M_{CH4}}{M_{He}}}b_{He}$
Javadpour [47]	$k_a = \frac{2r\mu M}{3\times10^3 RT\rho_{avg}^2}\sqrt{\frac{8RT}{\pi M}} + F\frac{r^2}{8\rho_{avg}}$	$F = 1 + \sqrt{\left(\frac{8\pi RT}{M}\right)}\frac{\mu}{p_{avg}r}\left(\frac{2}{\alpha} - 1\right)$
Tang, et al. [48]	$k_a = k_\infty\left(1 + \frac{A}{p} + \frac{B}{p^2}\right)$	$A = \frac{8\mu}{D}\sqrt{\frac{\pi R_g T}{2M}}C_1 B = \frac{8\pi\mu^2}{D^2}\frac{R_g T}{2M}C_2$
Beskok, Karniadakis [49]	$k_a = k_\infty(1 + \alpha Kn)\left(1 + \frac{4Kn}{1 - bKn}\right)$	$\alpha = \alpha_0\frac{2}{\pi}\tan^{-1}\alpha_1 Kn^{\alpha 2}$
Civan [50]		$\frac{\alpha_0}{\alpha} - 1 = \frac{A}{Kn^B}$

$$q(h)=\frac{\pi h^4}{128\mu}\left(1+\frac{8\lambda}{h}\right)\frac{\Delta p_m}{L_\tau(h)}+\frac{h^3}{6p}\sqrt{\frac{2\pi RT}{M_g}}\frac{\Delta p_m}{L_\tau(h)} \tag{14}$$

The pore diameter of the coal matrix spans from micrometre to nanometre. Previous studies reported that the PSD of the coal matrix exhibits natural self-affinity and can be represented with a fractal scaling law [14,53,54]. In a REV of coal, the matrix is assumed to be a bundle of capillary tubes with different cross-sectional areas, as shown in Fig. 3.

The fundamental law governing the pore numbers and PSD parameters is written as [26]:

$$N(H\geqslant h)=(h_{\max}/h)^{D_h} \tag{15}$$

where N is the cumulative number of pores with a diameter larger than the minimum value in the coal matrix, H is the characteristic value of the pore diameter, h and $h_{\max}$ are the pore diameter and maximum pore diameter, respectively, D_h is the fractal dimension for PSD, and$0<D_h<2$. The infinitesimal increment in the pore number to pore size change can be derived through differentiating both sides of Eq. (15):

$$-dN=D_h(h_{\max})^{D_h}h^{-(D_h+1)}dh \tag{16}$$

According to Eq. (15), when the pore diameter reaches a minimum value, the cumulative number of pores in the whole range of the coal matrix can be formulated as

$$N_t(H\geqslant h_{\min})=(h_{\max}/h_{\min})^{D_h} \tag{17}$$

where $h_{\min}$ is the minimum pore diameter and N_t is the total number of pores. Based on Eqs. (16) and (17), we can further write [26,55]:

$$-\frac{dN}{N_t}=h(h_{\min})^{D_h}h^{-(D_h+1)}dh=f(h)dh \tag{18}$$

where $f(h)$ is the probability density function of the PSD. The correlation between the fractal dimension and porosity is expressed as:

$$D_h=d-\frac{\ln(\phi)}{\ln(h_{\min}/h_{\max})} \tag{19}$$

As shown in Fig. 3, L_0 is the characteristic length of REV and L_τ is the tortuous flow length, which is formulated as:

$$L_\tau=L_0^{D_T}h^{1-D_T} \tag{20}$$

where D_τ is the fractal dimension of tortuosity of flow path length, and $1<D_\tau<2$ in two Euclidean dimensions. According to the distribution of pore size given in Eq. (11), the total cross-sectional area of pores in REV can be integrated as:

$$A_p=-\int_{h_{min}}^{h_{max}}\frac{1}{4}\pi h^2dN=\int_{h_{\min}}^{h_{\max}}\frac{1}{4}\pi h^2D_hh_{\max}^{D_h}h^{-(D_h+1)}dh$$
$$=\frac{\pi D_hh_{\max}^2}{4(2-D_h)}\left[1-\left(\frac{h_{\min}}{h_{\max}}\right)^{2-D_h}\right] \tag{21}$$

Based on the definition of porosity, the cross-sectional area can be obtained from:

$$A=\frac{A_p}{\phi_m}=\frac{\pi D_hh_{\max}^2}{4\phi_m(2-D_h)}\left[1-\left(\frac{h_{\min}}{h_{\max}}\right)^{2-D_h}\right] \tag{22}$$

Therefore, for the accumulative flux of REV, the total flux can be obtained through:

$$Q=-\int_{h_{\min}}^{h_{\max}}q(h)dN=\frac{k_m}{\mu}A\frac{\Delta p}{L_0} \tag{23}$$

The modified gas flux can be obtained by combining Eqs. (14), (21), (22), and (23) to give:

$$k_m=\frac{\pi}{128}\frac{1}{L_0^{D_T+1}}\frac{D_h}{3+D_T-D_h}h_{\max}^{3+D_T}\left(1+\frac{8\mu(3+D_T-D_h)}{h_{\max}p_m(2+D_T-D_h)}\sqrt{\frac{\pi R_gT}{2M_g}}\right)$$
$$+\sqrt{\frac{2\pi RT}{M_g}}\frac{\mu D_h}{(2+D_T-D_h)}\frac{h_{\max}^{2+D_T}}{6p_mL_0^{D_T+1}} \tag{24}$$

The improved permeability model incorporates PSD and the slippage correction factor, which is correlated with porosity, fractal dimension and maximum pore diameter. As in gas injection or gas depletion processes, the above parameters change dynamically. The evolution equation with pore pressure is developed in subsequent subsections. The evolution of matrix porosity is calculated by [37]:

$$\phi_m=\phi_{m0}+\alpha\left[\varepsilon_v+\frac{p_m-p_0}{K_s}+\frac{\varepsilon_LP_L(p_0-p_m)}{(p_0+P_L)(p+P_L)}\right] \tag{25}$$

According to Eq. (24), the matrix permeability depends on the maximum pore diameter. Due to the multi-scale distribution of the pore diameter, there is no universal approach to calculating the change in pore diameter under effective stress, and Table 2 provides a brief review of the formulas used to determine pore diameter evolution.

The pore volume change ratio can also be rewritten as [37,65]:

$$\frac{V_p-V_p}{V_p}=-\frac{1}{K_p}\left(\Delta\sigma-\left(1-\frac{K_p}{K_s}\right)\Delta p_m\right)+\Delta\varepsilon_s \tag{26}$$

According to Eq. (3) and the definition of Biot's coefficient, the expression below can be deduced as follows [66]:

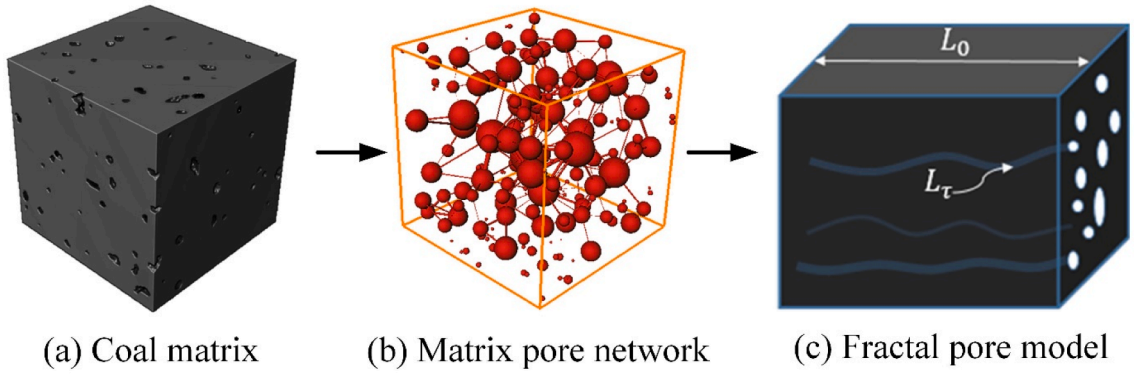

Fig. 3. Schematic illustrations of the fractal model of coal matrix: (a) original coal matrix structure; (b) pore network with different pore throat; (c) the fractal capillary tube-based coal matrix model.

Table 2
Pore radius change model under effective stress.

Reference.	Model	Description
Lei, et al. [56]	$r = r_0\left\{1-4\left[\frac{3\pi(1-\nu^2)p_{eff}}{4E}\right]^{2/3}\right\}$	p_{eff} is the effective stress
Tan, et al. [57]	$\lambda_p = \sqrt{\frac{\sqrt{3}-2F_c}{4F_p}}\left[1-\left(\frac{-\sigma}{E}\right)^{1/n}\right]\lambda_{c0}$	F_c and F_p are the formation factors
Lei, et al. [58]	$r = r_0 - \frac{1-\nu}{E}\frac{r_0^3 p_{eff}}{r_1^2-r_0^2} - \frac{1+\nu}{E}\frac{r_0 r_1^2 p_{eff}}{r_1^2-r_0^2}$	r_1 is the outer radius
Si, et al. [59]	$r = r_0\left(1+\frac{\alpha}{\phi K}(\Delta\sigma-\Delta p)-\Delta\varepsilon_s\right)^{-1/3}$	α is the Biot coefficient, $\Delta\varepsilon_s$ is the sorption strain
Lv, et al. [60]	$r = r_0\left\{1-\frac{2(1-\nu^2)}{E}\left[\sigma-\frac{1}{2(1-\nu)}p\right]\right\}$	ν is Poisson's ratio
Wu, et al. [61]	$r = r_0(p_e/p_0)^{0.5(q-s)}$	p_e is the effective stress, q and s are the porosity coefficients
Cao, et al. [62]	$r = r_0\exp\left\{\left(\frac{1}{K}-\frac{1}{K_p}\right)[(\Delta\sigma-\Delta p)]\right\}$	K_p is the pore bulk modulus
Zhang, et al. [63]	$r = r_0\left[\frac{1-(\sigma/p_1)^m}{1-(\sigma_0/p_1)^m}\right]^{1.5}$	p_1 is the stiffness parameter, m is the roughness parameter
Tang, et al. [64]	$r = r_0\exp\left[-c_m\left(\sigma_c-\chi p_f\right)/4\right]$	c_m is compressibility, χ is Biot coefficient

$$\Delta\overline{\sigma}-\Delta p_m = -K\left(\Delta\varepsilon_v+\frac{\Delta p_m}{K_s}-\Delta\varepsilon_s\right) \tag{27}$$

Substituting Eq. (27) into (26) yields:

$$\frac{V_p}{V_p} = \frac{A_pL_0}{A_pL_0} = 1+\frac{\alpha}{\phi_m}\left(\Delta\varepsilon_v+\frac{\Delta p_m}{K_s}-\Delta\varepsilon_s\right)-\frac{\Delta p}{K_s}+\Delta\varepsilon_s \tag{28}$$

In this study, under the 2D case, the$V_p = A_p$, combining Eq. (28) and (21) yields

$$\frac{\frac{D_h h_{\max}^2}{(2-D_h)}\left[1-\left(\frac{h_{\min}}{h_{\max}}\right)^{2-D_h}\right]}{\frac{D_{h0}h_{\max0}^2}{(2-D_{h0})}\left[1-\left(\frac{h_{\min0}}{h_{\max0}}\right)^{2-D_{h0}}\right]} = 1+\frac{\alpha}{\phi_m}\left(\Delta\varepsilon_v+\frac{\Delta p_m}{K_s}-\Delta\varepsilon_s\right)-\frac{\Delta p_m}{K_s}+\Delta\varepsilon_s \tag{29}$$

Because $h_{\min}\gg h_{\max}$, Eq. (29) can be simplified to:

$$\frac{h_{\max}^2}{h_{\max0}^2} = \left[1+\frac{\alpha}{\phi_m}\left(\Delta\varepsilon_v+\frac{\Delta p_m}{K_s}-\Delta\varepsilon_s\right)-\frac{\Delta p_m}{K_s}+\Delta\varepsilon_s\right]\frac{2-D_h}{2-D_{h0}}\frac{D_{h0}}{D_h}\frac{1-\phi_{m0}}{1-\phi_m} \tag{30}$$

Based on Eq. (30), the maximum pore diameter of fractal pores can be obtained from:

$$h_{\max} = h_{\max0}\sqrt{\left[1+\frac{\alpha}{\phi_m}(S-S_0)-\frac{p_m-p_0}{K_s}+\varepsilon_s-\varepsilon_{s0}\right]\frac{2-D_h}{2-D_{h0}}\frac{D_{h0}}{D_h}\frac{1-\phi_{m0}}{1-\phi_m}} \tag{31}$$

where the$S = \varepsilon_v+\frac{p_m}{K_s}-\varepsilon_s$,$S_0 = \varepsilon_{v0}+\frac{p_0}{K_s}-\varepsilon_{s0}$ D_{h0} is the initial value of the fractal dimension while D_h is the fractal dimension under effective stress.

2.4. Dynamic permeability for coal fractures

The seepage capacity of the coal fracture networks is far higher than that of coal matrix.. The porosity and permeability of coal fracture is highly dependent on the fracture apertures, which evolve under impacts of effective stress and the matrix swelling/shrinkage. Apart from pores in the coal matrix, the fracture aperture also has fractal characteristics [67,68], as shown in Fig. 4.

According to cubic law, the flux flowing through fractures is calculated by:

$$q_f = -\frac{Wb^3}{12\mu}\frac{\Delta p}{L_{tf}} \tag{32}$$

where W is the fracture width, b denotes the fracture aperture and L_{tf} represents the tortuous flow length. According to Eq. (15) and (16),

$$-dN = D_h(h_{\max})^{D_h}h^{-(D_h+1)}dh \tag{33}$$

Therefore, the total flow flux through all fractures can be integrated as:

$$Q_f = \int_{b_{\min}}^{b_{\max}} q_f dN = \frac{W}{12\mu}\frac{D_b}{2+D_{tf}-D_b}\frac{\Delta p}{L_{tf}^{D_{tf}}}b_{\max}^{2+D_{tf}}\left(1-\beta^{2+D_{tf}-D_b}\right) \tag{34}$$

where $\beta = b_{\min}/b_{\max}$, macroscopically, when fluid flow through fractures, the total flow flux can be described with Darcy flow law, which is defined as:

$$Q_f = \frac{k_f A_f}{\mu}\frac{\Delta p}{L_{tf}} \tag{35}$$

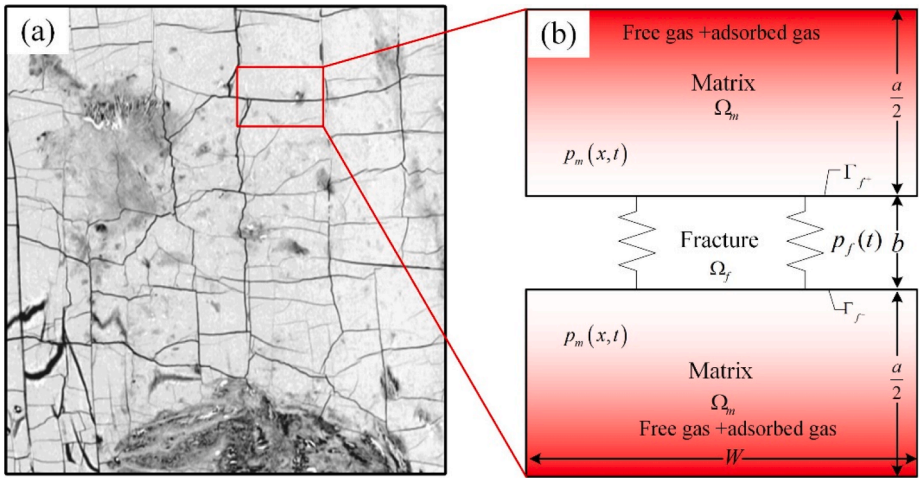

Fig. 4. Schematic illustrations of the representative volume with fractally distributed fracture: (a) the cross-section of coal REV perpendicular to flow direction; (b) single fracture and the adjacent matrix REV.

where A_f is the cross-section area of fracture REV, which is defined as$A_f = N_t(a+b)W$. As the fracture spacing is far larger than the fracture aperture$a \gg b$, the cross-section area of fracture REV can be simplified as$A_f = N_t aW$. Therefore, combining Eqs. (34) and (35), the equivalent fracture permeability can be deduced as:

$$k_f = \frac{D_b b_{\max}^{2+D_{tf}}\left(1-\beta^{2+D_{tf}-D_b}\right)}{12(a+b)\left(2+D_{tf}-D_b\right)L_{tf}^{D_{tf}-1}} \tag{36}$$

According to Fig. 2, when the fracture aperture is smaller than 100 μm, the slip flow can be pronounced and should not be neglected. Therefore, the fractal-based Klinkenberg coefficient is analogous to the expression in the coal matrix, and the modified permeability for fractures is expressed as:

$$k_f = \frac{D_b b_{\max}^{2+D_{tf}}\left(1-\beta^{2+D_{tf}-D_b}\right)}{12(a+b)\left(2+D_{tf}-D_b\right)L_{tf}^{D_{tf}-1}}\left(1+\frac{8\mu\left(3+D_{tf}-D_b\right)}{b_{\max}p_f\left(2+D_{tf}-D_b\right)}\sqrt{\frac{\pi R_g T}{2M_g}}\right) \tag{37}$$

In the above equation, the major variables under effective stress are maximum pore diameter and the fractal dimension of apertures. The equation linking fractal dimension and porosity is analogous to the fracture length because of the linear relationship between fracture length and fracture aperture, and the fractal dimension of fracture aperture can be formulated as [69]:

$$D_b = d - \ln\left(\phi_f\right)/\ln(b_{\min}/b_{\max}) \tag{38}$$

where b_0 is the initial fracture aperture, ϕ_{f0} is the initial fracture porosity, it is assumed that the maximum fracture ratio is equivalent to the porosity ratio. According to the study of Wu, et al. [70], the fracture porosity is determined by:

$$\frac{\phi_f}{\phi_{f0}} = \frac{b_{ave}}{b_{ave0}} = 1 - \frac{3}{\phi_{f0}+\frac{3K_f}{K}}\left(\frac{\varepsilon_L \Delta P_m}{P_L+\Delta P_m} - \varepsilon_v\right) \tag{39}$$

where b_{ave} is the average fracture aperture, b_{ave0} is the initial average aperture, K_f is the fracture stiffness, K is the bulk modulus. The relationship between average fracture aperture and maximum aperture is expressed as [71]:

$$b_{ave} = \int_{b_{\min}}^{b_{\max}} b{\cdot}f(b)\mathrm{d}b = \frac{D_b b_{\max}}{D_b-1}\left[\frac{b_{\min}}{b_{\max}} - \left(\frac{b_{\min}}{b_{\max}}\right)^{D_b}\right] \tag{40}$$

As the $b_{\min}/b_{\max}$ is assumed constant and$b_{\min} \ll b_{\max}$, the maximum aperture ratio can be derived as:

$$\frac{b_{\max}}{b_{\max 0}} = \frac{b_{av}}{b_{av0}}\frac{D_b}{D_{b0}}\frac{D_{b0}-1}{D_b-1} \tag{41}$$

Besides, according to our previous study [72], the fracture spacing and aperture under effective stress can be calculated by:

$$a+b = (a_0+b_0)\left(1-\frac{\Delta\sigma-\Delta p}{K}\right) \tag{42}$$

where a_0 and b_0 are the initial fracture spacing and fracture aperture, The total permeability of coal is given as [73,74]:

$$k = k_m + k_f \tag{43}$$

$$\frac{k}{k_0} = \frac{k_{m0}}{k_{m0}+k_{f0}}\frac{k_m}{k_{m0}} + \frac{k_{fo}}{k_{m0}+k_{f0}}\frac{k_f}{k_{f0}} \tag{44}$$

3. Model verification

Based on the preceding fractal-based matrix permeability and fracture permeability, the gas flow filed and coal deformation can be fully coupled. The whole set of coupled PDE equations proposed in the preceding sections are implemented in COMSOL MULTIPHYSICS, which is a commercial PDE solver. The dual fractal-permeability model was verified using the field data from Fairway well of San Juan Basin (Fruitland coal seam) [75]. To justify the advancement of the proposed model, P-M model [76], S-D model [77] and C-B model [38] were selected to conduct comparative analysis because the three models are based on the assumption of uniaxial strain condition. The simulation model is shown in Fig. 5(a), with a size being 50 m × 50 m and a well radius is 0.1 m in the corner of the physical model. The initial reservoir pressure is 10 MPa while the constant bottom-hole pressure is 0.1 MPa. Other parameters are the same as the values used in the experimental verification shown in Table 3. The basic assumptions of the reservoir simulation associated with the boundary condition are the following: (1) constant overburden stress at the top boundary; (2) the wellbore pressure is applied at the boundary of the well; (3) the no-flow condition is applied at other boundaries except for the well boundary. Fig. 5(b) compares the total permeability evolution between the simulated results, the field data and other three widely used models, indicating that modelling results agree well with the field data and show a better performance than the other classical models. The discrepancies between model results and field data demonstrate that the C-B model overestimated the effect of stress. P-M model and S-D model can predict permeability evolution partially, but the accuracy is significantly lower than the proposed model. It can be noted that the permeability increases when the reservoir pressure declines, which is because matrix shrinkage counteracts the compaction caused by the elevated effective stress. The pore pressure distribution of matrix and fracture are presented in Fig. 6 and Fig. 7 at different times. It can be seen that the fracture pressure declines faster than the matrix pressure. Fig. 8 presents the stress distributions at 10 days and 100 days.

4. Sensitivity analysis and discussion

4.1. Contributions of different flow mechanisms to matrix permeability

The flow regimes in coal matrix are mainly composed of slip flow and Knudsen diffusion according to Fig. 9. The variation of microstructure in the coal matrix can change the significance of each flow regime. To study the impacts of microstructure parameters on the contribution of Knudsen diffusion and slip flow, firstly, three sets of maximum pore diameters (h_{max0}) are adopted to perform sensitivity analysis. As shown in Fig. 9, with gas depletion in the coal seam reservoir, the proportion of slip flow decreases while the proportion of Knudsen diffusion increases gradually. For the base case with $h_{max0} = 500$ nm, the contribution ratio of slip flow to total apparent matrix permeability in the initial stage is 95 %, as shown in Fig. 9(a). However, when the final equilibrium state is achieved, the corresponding value drops to 40 %. By contrast, the contribution ratio of Knudsen diffusion increases from 5 % to 60 % when the pressure declines from 5 MPa to 0.1 MPa, as shown in Fig. 9(b). When the maximum pore diameter increases, the contribution ratio of slip flow is uplifted at the same reservoir pressure because the average pore radius is increased. Besides, the sensitivity of the contribution ratio to the fractal dimension of PSD in the coal matrix is also studied, as shown in Fig. 10. It can be observed that the fractal dimension has a marginal effect on the evolution of the flow regime. When the fractal dimension increases, the contribution ratio of slip flow experiences a slight decrease and the contribution ratio of Knudsen diffusion has a minor rise.

The flow in the coal matrix in some studies is assumed as pure diffusion or Darcy flow is not appropriate, which cannot reflect the true situation. Although some previous studies [78,79] have evaluated the importance of non-Darcy flow in coal matrix, the impacts of the heterogeneous structure are not incorporated. Accordingly, the advantage of the proposed model is that it replicates the heterogeneous structure and includes multiple flow regimes. Overall, the structure of the coal matrix is highly heterogeneous and the pore size spans several

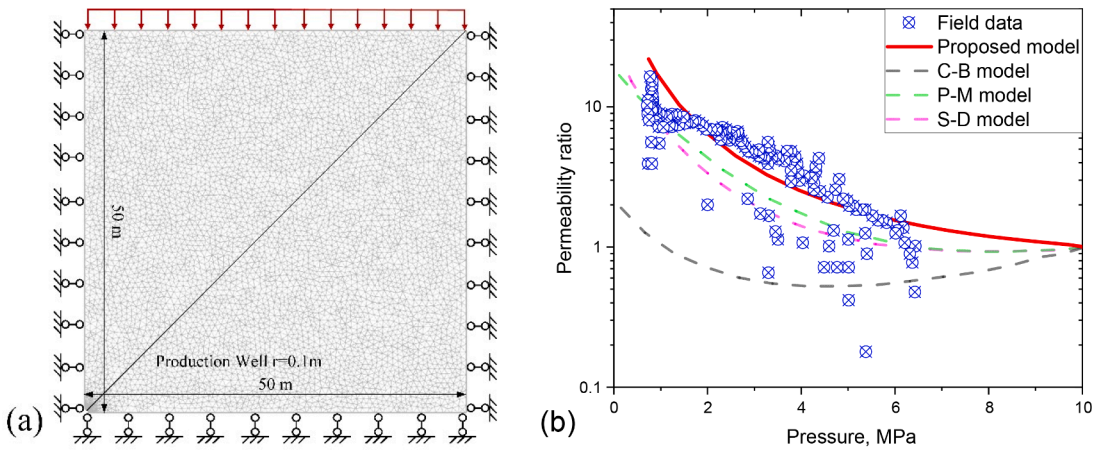

Fig. 5. Schematic illustration of the simulation model for field-scale.

Table 3
The input parameters for the field verification.

Parameter Symbols	Physical meaning	Value	Unit
T	Temperature	300	K
ϕ_{m0}	Initial porosity of matrix	0.02	—
ϕ_{f0}	Initial porosity of fracture	0.03	—
E	Young's modulus of Coal	3713	MPa
E_s	Young's modulus of coal grains	12,139	MPa
K_f	Fracture stiffness	0.3	GPa
ν	Poisson's ratio	0.33	—
ε_L	Langmuir strain constant	0.03	—
p_L	Langmuir pressure constant	4.5	MPa
ρ_s	Density of coal	1250	kg/m^3
μ	Methane viscosity	1.22×10^{-5}	Pa*s
h_{min}	Minimum pore diameter	5	nm
h_{max}	Maximum pore diameter	500	nm
D_T	Fractal dimension of pore tortuosity	1.4	—
D_h	The initial fractal dimension of PSD	1.15	—
b_{min}	Minimum fracture aperture	0.4	μm
b_{max}	Maximum fracture aperture	20	μm
D_{tf}	Fractal dimension of fracture tortuosity	1.4	—
D_b	initial fractal dimension of fracture	1.1	—

magnitudes. According to the fractal-based matrix permeability shown in Eq. (24), gas flow in the matrix is highly dependent on the microstructure, including the maximum pore diameter and fractal dimension.

4.2. Impacts of matrix heterogeneity on permeability evolution

The heterogeneity of the coal matrix plays a pivotal role in the absolute permeability and permeability evolution during gas depletion. In this study, the structural heterogeneity of the coal matrix primarily refers to the fractal dimension of PSD (D_h), and fractal dimension of pore tortuosity (D_T). Both of these heterogeneous parameters affect the porosity and permeability directly. It is essential to understand the impacts of these heterogeneities on permeability evolution under the condition that gas flow and geomechanics are coupled. We set up a base case according to the simulation results in the previous field verification, where the fractal dimension of PSD is$D_{h0} = 1.15$, the fractal dimension of tortuosity is $D_T = 1.4$ and the maximum pore diameter is$h_{max0} =$ 500nm. Based on that, three sets of fractal dimensions of PSD ($D_{h0} =$ 1.15, $D_{h0} = 1.35$ and $D_{h0} = 1.5$), pore tortuosity ($D_T = 1.2$, $D_T = 1.4$ and $D_T = 1.6$) and maximum pore diameter ($h_{max0} =$ 300nm, $h_{max0} =$ 500nm and $h_{max0} =$ 700nm) are used to conduct sensitivity analysis. The initial permeability and the corresponding pore number for the various cases are presented in Fig. 11(a) and (b).

As presented in Fig. 12(a), the initial fractal dimension plays a significant role in the permeability evolution of the coal matrix. With the depletion of gas, coal permeability increases in all cases, which can be attributed to the fact that the shrinkage-induced pore diameter

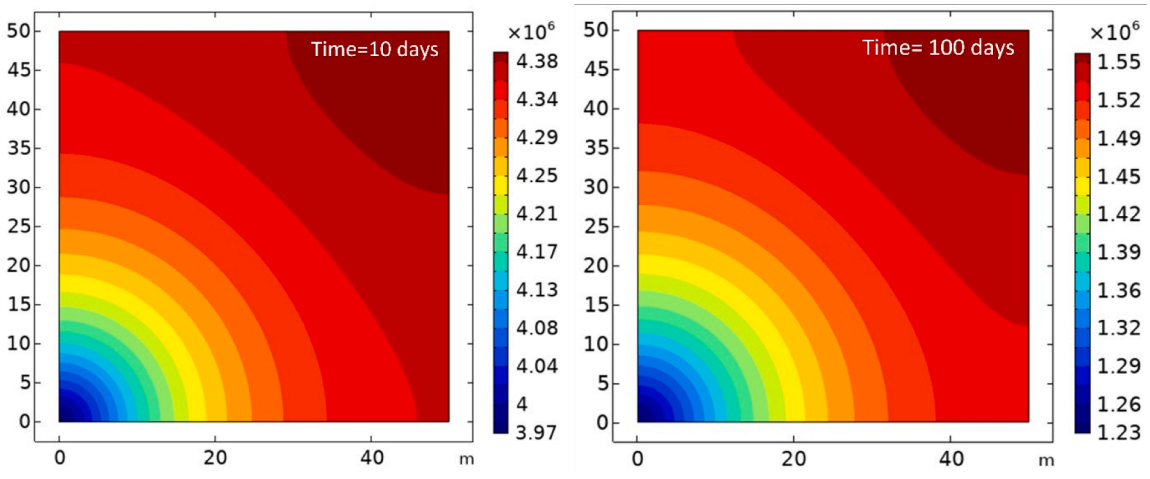

Fig. 6. Pressure distribution of matrix system after 10 days and 100 days of production.

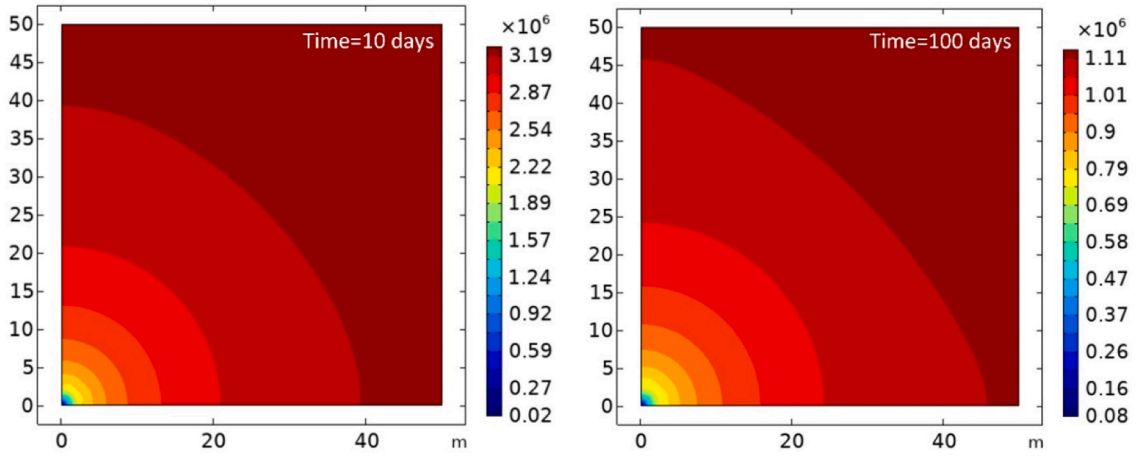

Fig. 7. Pressure distribution of fracture system after 10 days and 100 days of production.

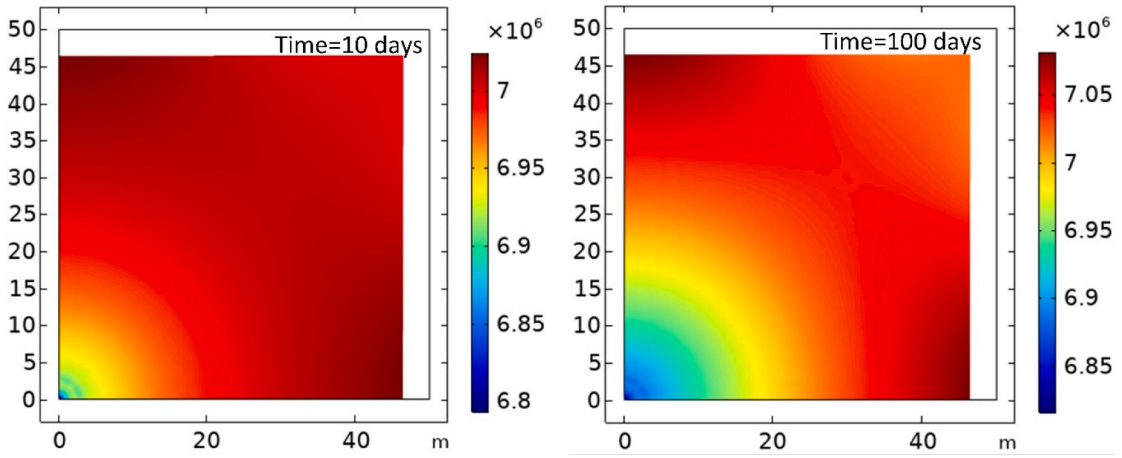

Fig. 8. Evolutions of Von Mise stress after 10 days and 100 days of production.

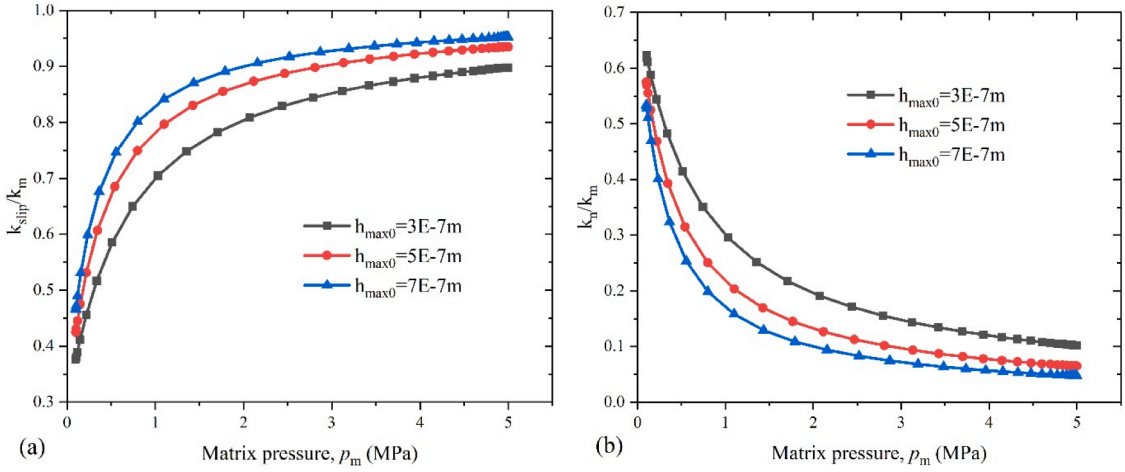

Fig. 9. Impacts of maximum pore diameter on the contribution ratios of various flow mechanisms to total matrix permeability.

increment and the reinforced slip flow override the pore diameter contraction resulting from the rising of the effective stress. Moreover, a smaller initial fractal dimension (initial porosity) indicates a greater increase in magnitudes. The evolution of porosity and maximum pore diameter are inversely proportional to initial porosity, as expressed in Eqs. (27) and (32). When the simulation time reaches 1×10^8s, there is an almost a 7-fold increase in the permeability when the initial fractal dimension is 1.15. By contrast, when $D_{h0} = 1.35$ and$D_{h0} = 1.5$, the final permeabilities are 6 and 5.5 times of initial permeability. Consequently, the fracture permeability with a smaller fractal dimension of PSD in the matrix experiences a more rapid increase, as shown in Fig. 12(b). However, the variation of the initiative D_h does not alter the final value

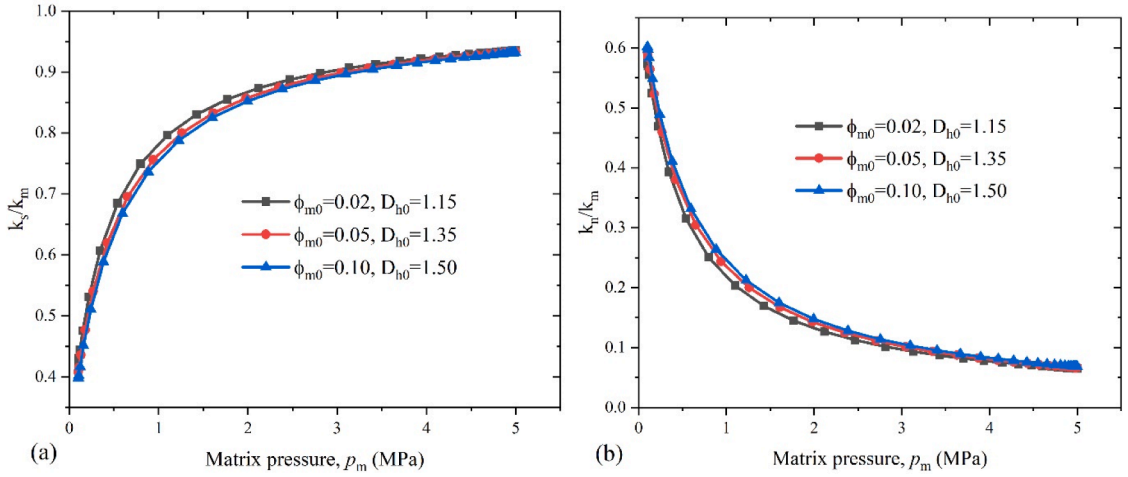

Fig. 10. Impacts of fractal dimension on the contribution ratios of various flow mechanisms to total matrix permeability.

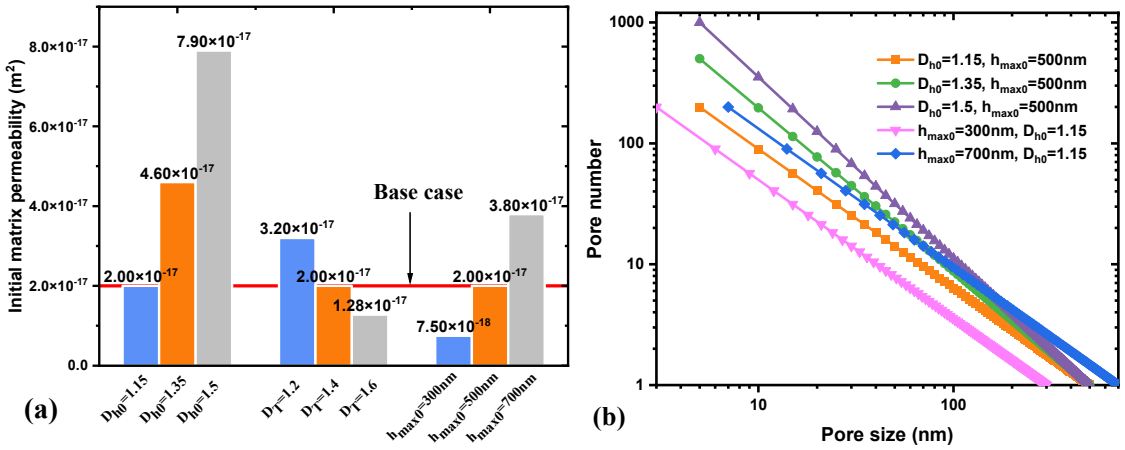

Fig. 11. (a) Initial matrix permeability for the various fractal parameter, and (b) the corresponding pore number for various fractal dimensions and maximum pore diameter.

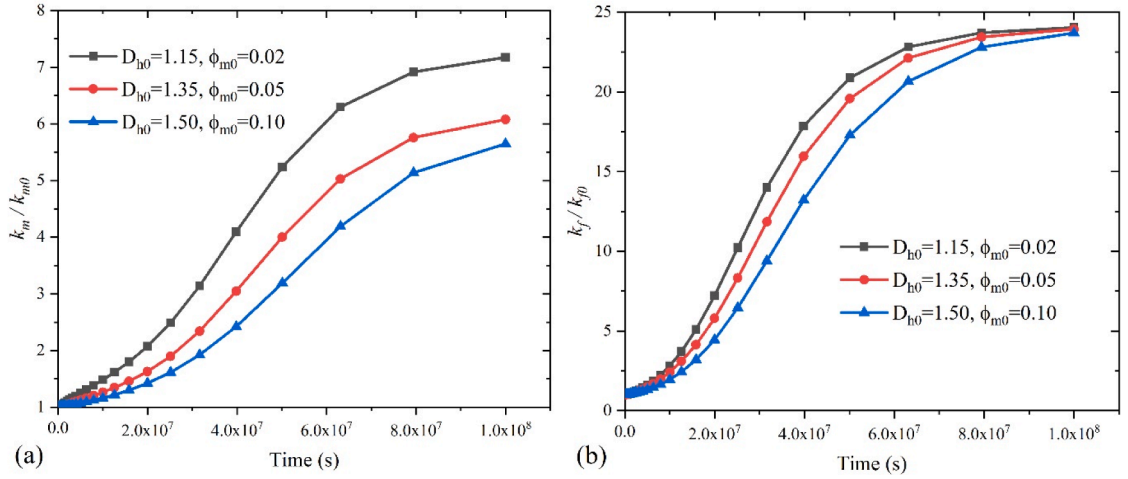

Fig. 12. Impacts of matrix fractal dimension on permeability evolutions.

of fracture permeability, and the fracture permeability for all three cases is 24 times of initial value. As the fractal dimension represents the heterogeneity of matrix microstructure, it can be concluded that when the matrix structure is more heterogeneous, the matrix permeability is less sensitive to effective stress.

Apart from the fractal dimension of PSD, the tortuosity of pores in the coal matrix can affect the permeability by increasing the flow length and retarding gas flow. Fig. 13 presents the permeability evolution with

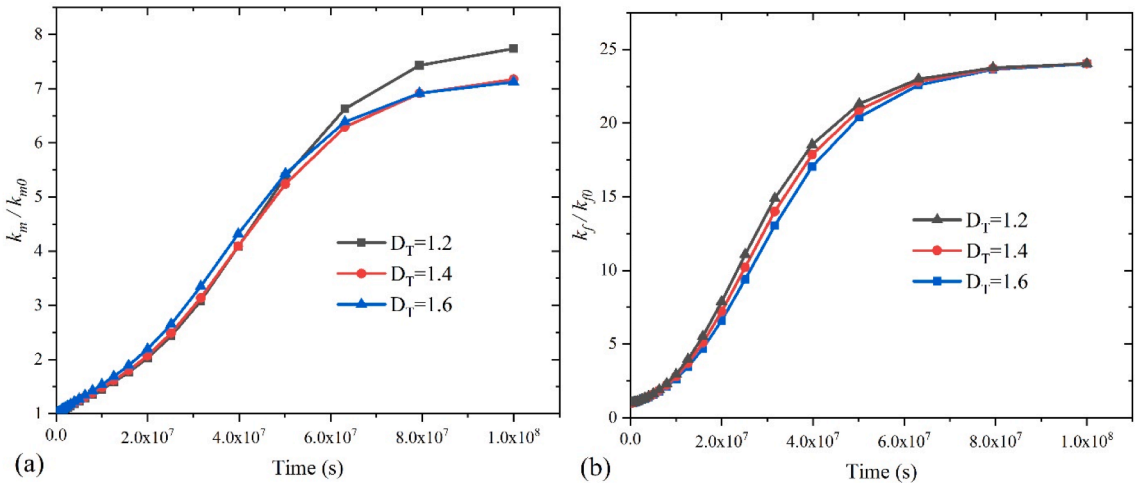

Fig. 13. Permeability evolution for the various fractal dimension of tortuosity.

different fractal dimensions of tortuosity. In the initial stage, the smaller fractal dimension of tortuosity indicates higher initial matrix permeability. When the fractal dimension of tortuosity is 1.2, the permeability experiences an 8-fold increase when the final equilibrium is achieved. For the remaining cases with $D_T = 1.4$ and$D_T = 1.6$, the corresponding permeability experience an approximately 7-fold increase at the same production time. The results suggest that tortuosity has an adverse effect on permeability evolution. Correspondingly, the fracture permeability for the case with a larger fractal dimension of tortuosity increases more rapid due to the larger matrix permeability and the mass transfer rate according to Eqs. (9) and (24).

Maximum pore diameter is another factor that affects the absolute permeability and permeability evolution during gas depletion. In this study, it is assumed that the h_{min}/h_{max} remains constant, which means that the maximum pore diameter represents the overall pore distribution. Eq. (24) suggests that the matrix permeability evolution is strongly dependent on the dynamic change of the maximum pore diameter. Fig. 14 illustrates both of the matrix and fracture permeability evolutions for three groups of maximum pore diameters. Whenh_{max0} = 700nm, the permeability increases 5 times when the final equilibriums state is achieved (The total production time is 1×10^8s). By contrast, when h_{max0} = 500 nm andh_{max0} = 300 nm, there is a 7-fold and 10-fold increase, respectively. Larger maximum pore diameter indicates larger initial matrix permeability but smaller final permeability. The reason for this phenomenon is the slippage coefficient in the slip flow term is inversely proportional to the maximum pore diameter. Therefore, smaller maximum pore diameter results in a more remarkable permeability increment because of more pronounced slip flow. At the same time, the variation of maximum pore diameter in coal matrix exhibits negligible effects on fracture permeability, as shown in Fig. 14 (b).

4.3. *Impacts of fracture heterogeneity in permeability evolution*

The fracture heterogeneity is controlled by the multiscale fracture aperture (D_b) and fracture tortuosity (D_{tf}) and various maximum aperture sizes. According to the fracture permeability shown in Eq. (37), the maximum aperture and fractal dimension are pressure-dependent. To further understand the impacts of these two factors on permeability evolution, various heterogeneous parameters are used to perform the simulation. In the base case, the fractal dimension of PSD is 1.1, the fractal dimension of tortuosity is 1.25 and the maximum aperture is 2 μm. Based on that, three sets of fractal dimensions of PSD ($D_{b0} = 1.1$, $D_{b0} = 1.25$ and $D_{b0} = 1.4$), pore tortuosity ($D_{tf} = 1.2$, $D_{tf} = 1.4$ and $D_{tf} = 1.6$) and maximum aperture ($b_{max0} = 1.5\mu m$,$b_{max0} = 2.0\mu m$ and $b_{max0} = 2.5\mu m$) are used to conduct sensitivity analysis. The initial fracture permeability for the various fractal parameters are presented in Fig. 15(a). In addition, the corresponding pore number for various fractal dimensions of aperture and maximum aperture is illustrated in Fig. 15(b).

The fracture aperture of coal is several magnitudes larger than the pore size in the coal matrix, which acts as the major flow path for gas

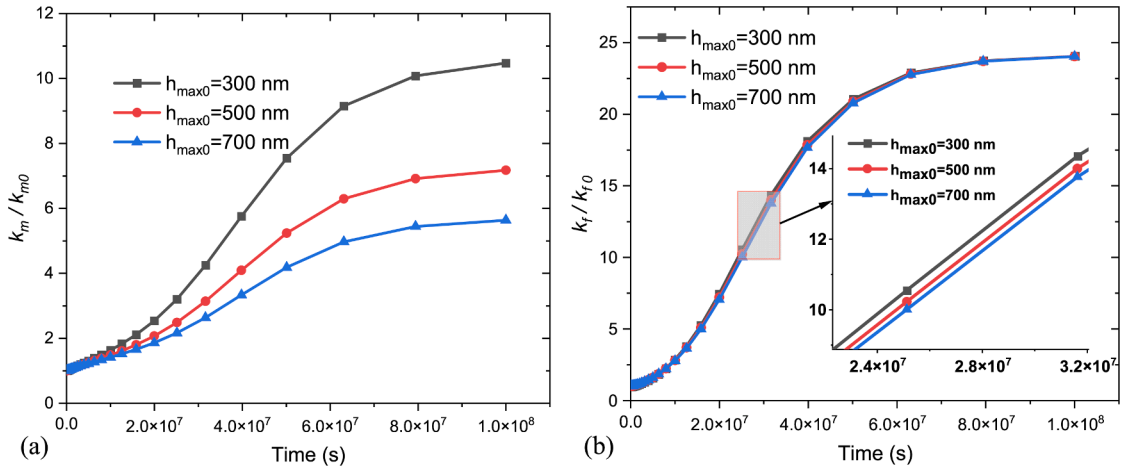

Fig. 14. Permeability evolution for various maximum pore diameter.

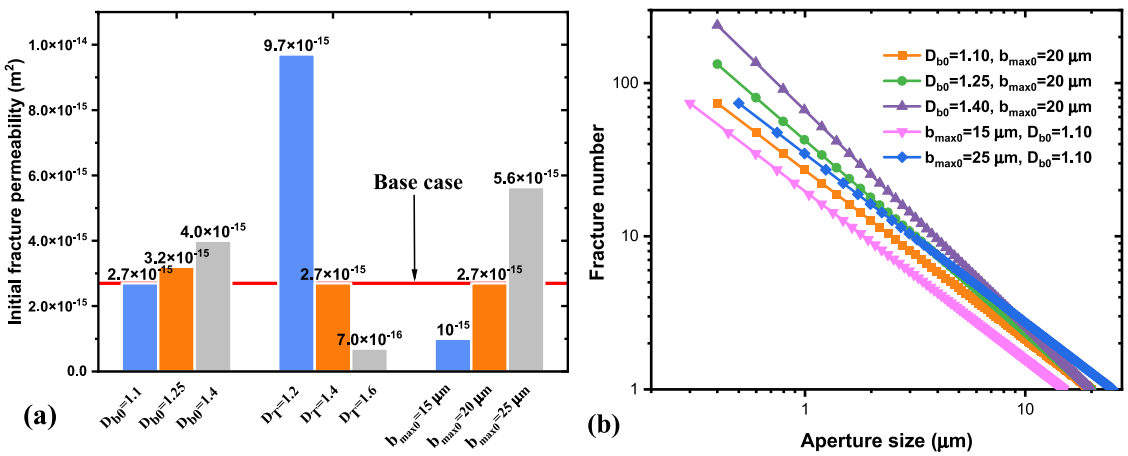

Fig. 15. (a) Initial fracture permeability for various fractal parameters, and (b) the corresponding fracture number for various fractal dimensions and maximum apertures.

flow. A wide distribution of fracture aperture can affect the absolute permeability and dynamic evolution substantially. Three sets of fractal dimensions of aperture ($D_{b0} = 1.1$, $D_{b0} = 1.25$ and $D_{b0} = 1.4$) are used to perform sensitivity analysis. As shown in Fig. 16(a), the smaller fractal dimension of the aperture indicates a faster increase in matrix permeability but does not change the final value. However, for the fracture permeability ratio, the smaller fractal dimension results in greater enhancement. When the final equilibrium is reached, the permeability for the case with $D_{b0} = 1.1$ experience a 24-fold increase. However, for $D_{b0} = 1.25$ and$D_{b0} = 1.4$, the permeability ratios decrease 18 times and 10 times, respectively, which is because the porosity and aperture ratio is inversely correlate correlated with fracture porosity and fractal dimension.

The importance of fracture tortuosity on permeability has been demonstrated by many scholars. However, the impact of tortuosity on the dynamic evolution under effective stress remains unclear. To address that, three sets of tortuosity, including$D_{tf} = 1.2$, $D_{tf} = 1.4$ and$D_{tf} = 1.6$, are adopted to conduct sensitivity analysis. According to Fig. 15, smaller fractal tortuosity indicates larger initial fracture permeability, which prompts the rapid mass transfer from coal matrix to fracture and the sequential matrix shrinkage. Consequently, the matrix permeability of the case with smaller tortuosity reaches the equilibrium state earlier, as shown in Fig. 17(a), but the final values of matrix permeability ratios are the same. However, it can be observed from Fig. 17(b) the fracture permeability for the larger tortuosity has larger permeability increment finally. The reason for this is the larger fractal dimension of tortuosity indicates larger exponent of the change range of maximum aperture, as illustrated in Eq. (37).

Fracture aperture decides the magnitudes of permeability directly and subtle changes of fracture aperture can affect the permeability substantially. The impact of effective stress and sorption-induced stress on permeability is primarily reflected in the variation of fracture aperture. Fig. 18 illustrates the evolutions for both matrix and fracture permeability when the maximum apertures are 1.5 μm, 2.0 μm and 2.5 μm, respectively. It is noticeable that a larger maximum aperture accelerates the growths of both matrix and fracture permeability. For the case with$b_{\max 0} = 2.5\mu m$, it takes 8×10^7s to reach the final equilibrium. However, when the maximum aperture decreases to 1.5 μm, the equilibrium time extends to 2×10^8s. It is worthwhile to mention that the final permeability for different maximum aperture is slightly different, which can be attributed to the slip flow that occurs in the fracture system. Overall, various maximum fracture aperture has a remarkable effect on the dynamic process but an insignificant effect on the incremental range during gas depletion. By contrast, the fractal dimension of pore size and tortuosity affects both the process and the final permeability ratio.

4.4. *Evolutions of microstructure and the impacts on slippage effect*

There are multitudes of stress-dependent permeability models to investigate the evolution of stress sensitivity. In these homogeneous models, the impacts of stress on the coal structure are mainly reflected

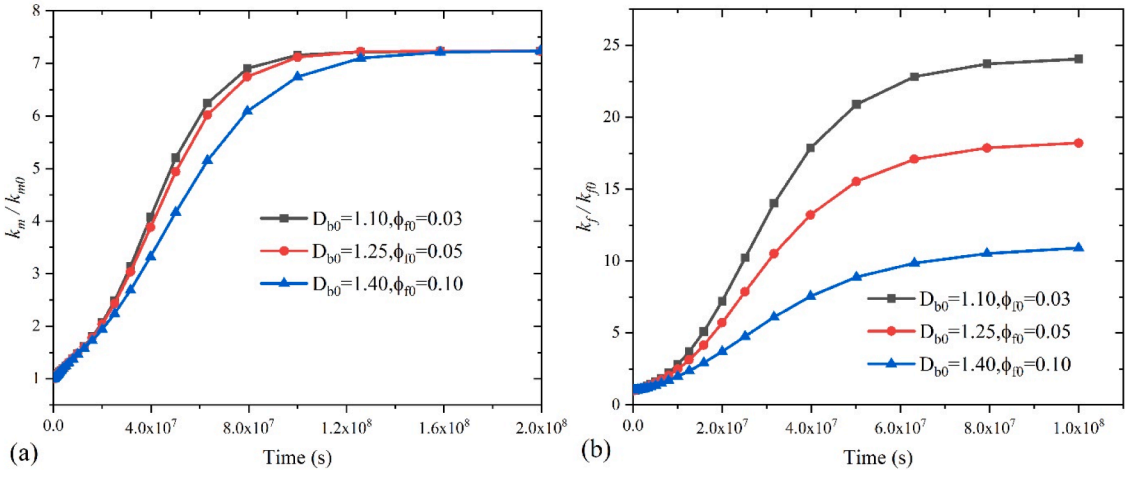

Fig. 16. Permeability evolutions for the various fractal dimension of fracture aperture.

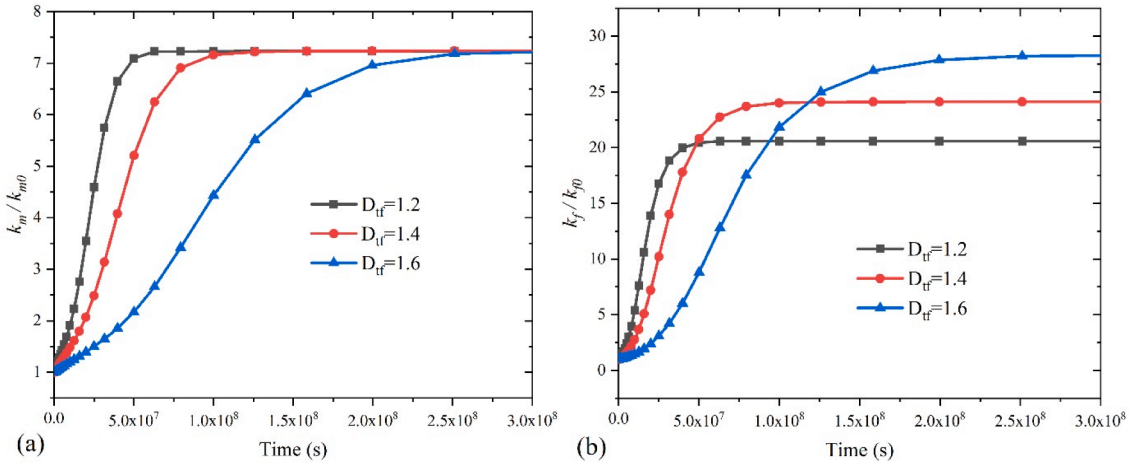

Fig. 17. Impacts of fracture tortuosity on permeability evolution.

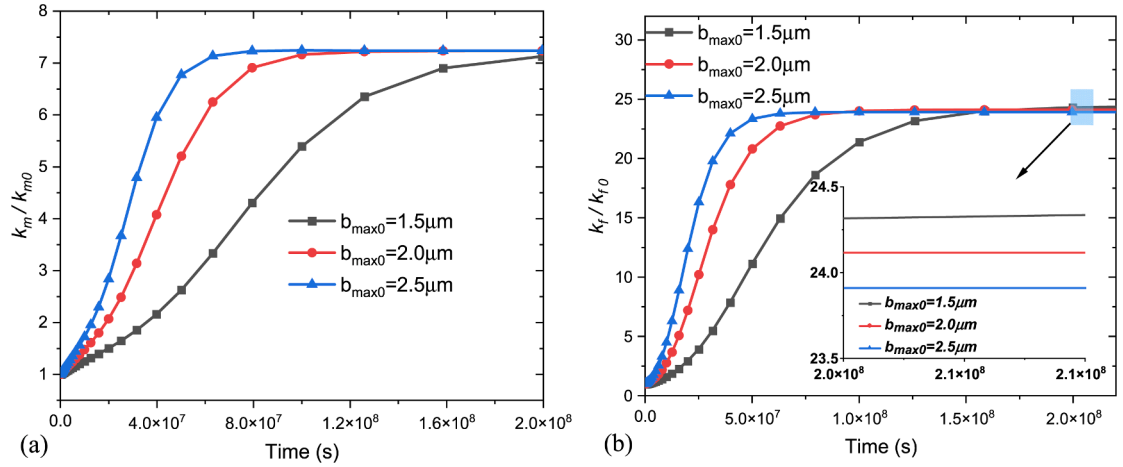

Fig. 18. Permeability evolution for various maximum fracture aperture.

through the evolution of porosity. However, the concrete evolution of heterogeneous structures cannot be captured. In our proposed fractal-based model, the impacts of effective stress and sorption-induced swelling stress on coal structure evolution are represented with the variation of maximum aperture, the fractal dimension of aperture distribution and fracture porosity. Evolutions of fractal dimensions of the pore (aperture) and the maximum pore size (fracture aperture size) are illustrated in Fig. 19(a) and (b), respectively. It can be noted that the fractal dimension of the matrix pore increases from 1.15 to 1.19 with the decline of matrix pressure from 5 MPa to 0.1 MPa. By contrast, the fractal dimension of fracture aperture increases from 1.1 to 1.32. Therefore, during gas depletion, the fracture aperture experiences a more dramatic change. As the fractal dimension represents the heterogeneity of coal structure. The more notable change of fracture aperture

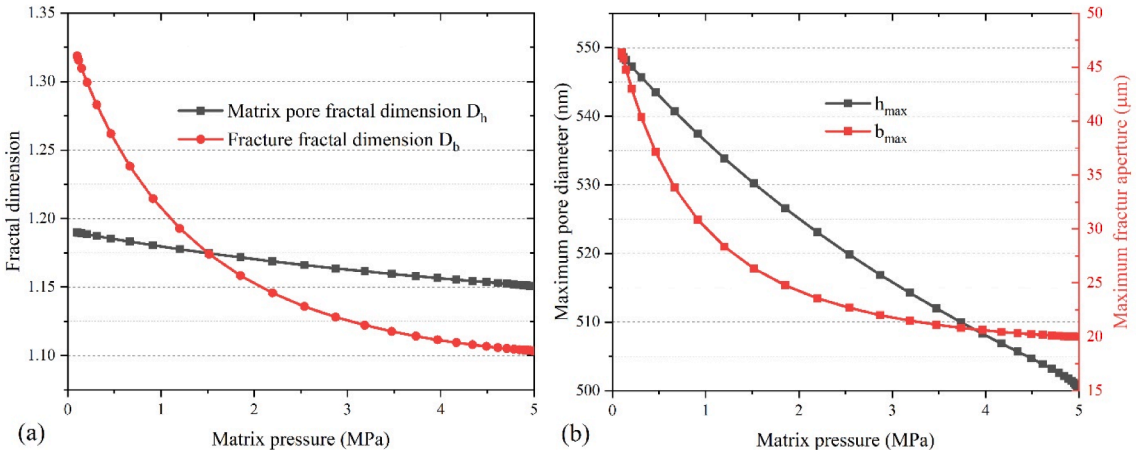

Fig. 19. Evolutions of fractal dimension and pore size.

distribution suggests that the fracture system becomes more heterogeneous. Besides, the maximum pore diameter in the coal matrix increases from 500 nm to 550 nm finally. By contrast, the maximum fracture aperture grows from 20 μm to 47 μm, increasing by 2.35 times.

The dynamic evolution of microstructure under effective stress and sorption-induced swelling affects the slip flow in the matrix as well as fracture. As shown in Fig. 20(a), with the decline of matrix pressure, the matrix permeability increases while the matrix slippage coefficient decreases. The slippage coefficient decreases from 0.44 MPa to 0.40 MPa approximately because of the enlargement of maximum pore size. The fracture slippage coefficient decreases from 0.011 MPa to 0.005 MPa when the final equilibrium is achieved, as shown in Fig. 20(b). It is demonstrated that the slippage in the coal matrix is more significant than that in fractures. According to previous experimental studies [80,81], the slippage coefficient of coal cleats increases when the effective stress increases because of the decreased aperture. However, in our study, with the depletion of gas from the coal seam reservoir, the slippage coefficient declines when the effective stress increases because the matrix shrinkages of pore and fracture offset the compaction caused by effective stress. Conclusively, both of the slippage coefficients in matrix and fracture tend to decline when the gas is depleted from the coal reservoir. Previous studies [46,82,83] have confirmed the importance of the slippage effect in coal, but the separate roles in matrix and fracture have not been explored. The advantage of the proposed model is the multiscale pore size and fracture aperture (critically important for slip flow) are incorporated using the fractal approach, which can simulate the true heterogeneous structure of coal.

4.5. Analysis of controlling factors for permeability

Gas depletion from a coal reservoir is a complex process that involves gas seepage and Knudsen diffusion in the coal matrix, slip flow in fractures, effective stress, and desorption-induced shrinkage. These effects are coupled through the evolution of permeability. However, the significance of each factor to permeability needs to be clarified. Fig. 21(a) illustrates the contributions of Terzaghi's effective stress, flow regime, and matrix shrinkage to matrix permeability. It can be noted that the black line represents the permeability evolution profile of the base case, which is referenced for other groups. First, when the Terzaghi effective stress is not considered, the permeability ratio is always larger than the referenced permeability, and the final permeability increases by a factor of 10. When the matrix shrinkage is not taken into account, there is a 6-fold increase. By contrast, when the Knudsen diffusion is neglected, the permeability ratio decreases significantly, with the final permeability increasing by a factor of three. If both the Knudsen diffusion and slip flow are excluded, the permeability ratio remains almost unchanged. Based on the matrix permeability evolution in various scenarios, it can be concluded that in a coal matrix, the effects of non-Darcy flow mechanisms are equally important. In many stress-dependent permeability models, the gas seepage in the matrix is oversimplified as Darcy flow, which cannot reflect the gas transport and the associated matrix shrinkage. We also compare the evolutions of matrix permeability calculated by the fractal-based model and the conventional cubic model ($k_m = k_{m0}\left(\phi_f/\phi_{f0}\right)^3$), as shown in Fig. 21(b). When the final equilibrium state is achieved, the matrix permeability of the cubic model increases by a factor of 1.7. It can be noted that the cubic model tends to underestimate the matrix permeability.

However, the slip flow becomes insignificant in the fracture network because of wider seepage channels, as shown in Fig. 22(a). There is a slight difference in the fracture permeability in the low-pressure stage for the cases with and without slip flow. Terzaghi's effective stress and matrix shrinkage are the dominant factors that affect fracture permeability evolution. When Terzaghi effective stress is not considered, the final fracture permeability can increase by a factor of 40. However, when the matrix is neglected, the fracture permeability shows a declining trend. Overall, compared with matrix permeability, fracture permeability evolution is primarily controlled by desorption-induced shrinkage and Terzaghi effective stress. Fig. 22(b) compares fracture permeability evolutions for this work and the cubic models. When the final equilibrium state is achieved, the fracture permeability of the cubic model increases by a factor of 13. There is a great gap between the cubic model and the fractal-based model, which indicates that the cubic model can underestimate the permeability because of the neglect of the role of multiscale fracture apertures on permeability evolution.

5. Conclusions

In this study, an effective stress-dependent dual-fractal permeability model is developed to couple gas flow and coal deformation. Then, the fully coupled model is upscaled to field scale to investigate the impacts of heterogeneous microstructure on permeability and permeability evolution quantitatively. The multiple flow mechanisms in matrix-fracture system are incorporated into the constitutive relations. Based on sensitivity analyses and model results, the following conclusions can be drawn:

(1) The fractally distributed pore-fracture size determines the significance of multiple flow mechanisms to gas flow. Larger maximum pore diameter and fractal dimension indicate a higher contribution ratio of Knudsen diffusion to total gas flux and permeability. By contrast, increases in pore-fracture size and fractal dimensions can compromise the impacts of slippage effects on apparent permeability.
(2) Fractal dimensions and pore-fracture size evolve with the variation of effective stress, which represent the dynamic evolutions of

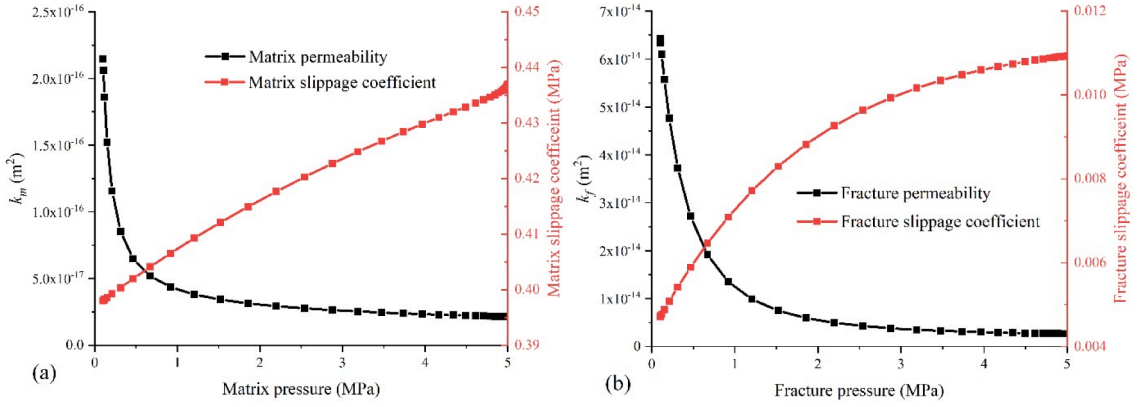

Fig. 20. Evolutions of slippage coefficient under effective stress.

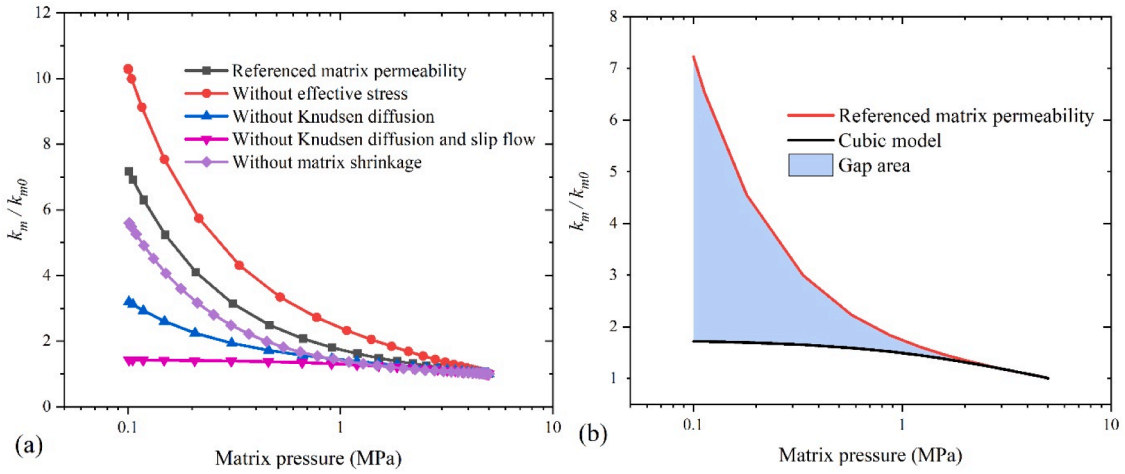

Fig. 21. (a) Influences of various factors on matrix permeability evolution; (b) comparison of matrix permeability calculated by the proposed model and cubic model.

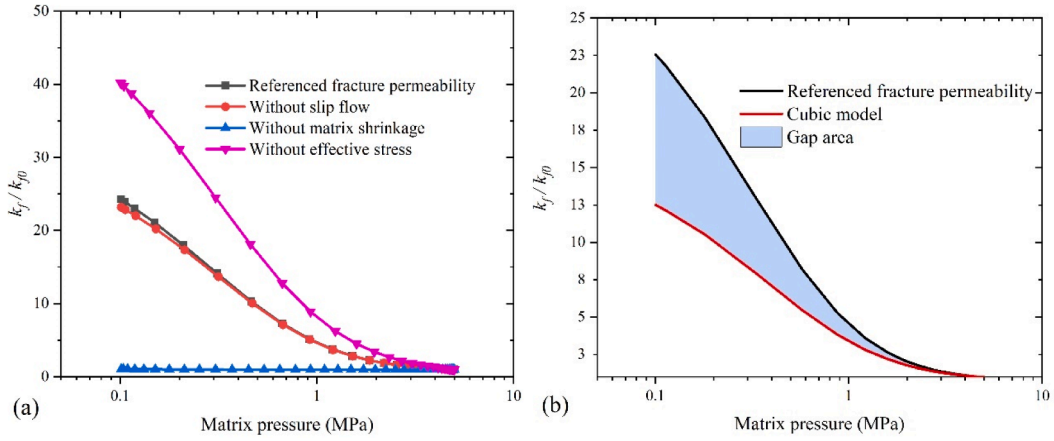

Fig. 22. (a) Influences of various factors on fracture permeability evolution; (b) comparison of fracture permeability calculated by the proposed model and cubic model.

coal microstructure under the impacts of stress. The desorption-induced shrinkage results in the increases in porosity, fractal dimensions of coal matrix-fracture system and maximum pore-fracture size, which intensify the structural heterogeneity. The fractal dimension of the fracture system shows a more significant growth than the matrix system.

(3) The permeability ratio increment of in coal matrix is dominated by the transition of flow regime, Terzaghi's effective stress and matrix shrinkage. However, fracture permeability ratio enhancement is controlled primarily by Terzaghi's effective stress and sorption-induced stress. The remarkable gaps on coal permeability evolutions between the proposed model and the widely used cubic model justifies the necessity of incorporating the fractally-distributed microstructure in coal permeability model.

Declaration of Competing Interest

The authors declare that they have no known competing financial interests or personal relationships that could have appeared to influence the work reported in this paper.

Data availability

Data will be made available on request.

Acknowledgements

This work is supported by the Australia Research Council under Grant DP200101293. The first author is supported by the China Scholarship Council (Grant number: 201706430057).

References

[1] Xia L, Yin Y, Yu X, Zheng Y. An approach to grading coalbed methane resources in China for the purpose of implementing a differential production subsidy. Pet Sci 2019;16(2):447–57.
[2] Connell LD, Lu M, Pan Z. An analytical coal permeability model for tri-axial strain and stress conditions. Int J Coal Geol 2010;84(2):103–14.
[3] Jasinge D, Ranjith PG, Choi SK. Effects of effective stress changes on permeability of latrobe valley brown coal. Fuel 2011;90(3):1292–300.
[4] Liu J, Chen Z, Elsworth D, Miao X, Mao X. Evolution of coal permeability from stress-controlled to displacement-controlled swelling conditions. Fuel 2011;90(10):2987–97.
[5] Wang M, Pan N. Numerical analyses of effective dielectric constant of multiphase microporous media. J Appl Phys 2007;101(11):114102.
[6] Wang GX, Wei XR, Wang K, Massarotto P, Rudolph V. Sorption-induced swelling/shrinkage and permeability of coal under stressed adsorption/desorption conditions. Int J Coal Geol 2010;83(1):46–54.
[7] Wei M, Liu J, Elsworth D, Li S, Zhou F. Influence of gas adsorption induced non-uniform deformation on the evolution of coal permeability. Int J Rock Mech Min Sci 2019;114:71–8.
[8] Zhu WC, Wei CH, Liu J, Xu T, Elsworth D. Impact of gas adsorption induced coal matrix damage on the evolution of coal permeability. Rock Mech Rock Eng 2013;46(6):1353–66.

[9] Chen D, Pan Z, Liu J, Connell LD. Characteristic of anisotropic coal permeability and its impact on optimal design of multi-lateral well for coalbed methane production. J Pet Sci Eng 2012;88:13–28.
[10] Pan Z, Connell LD. Modelling of anisotropic coal swelling and its impact on permeability behaviour for primary and enhanced coalbed methane recovery. Int J Coal Geol 2011;85(3–4):257–67.
[11] Wang K, Zang J, Wang G, Zhou A. Anisotropic permeability evolution of coal with effective stress variation and gas sorption: model development and analysis. Int J Coal Geol 2014;130:53–65.
[12] Cai Y, Liu D, Pan Z, Yao Y, Li J, Qiu Y. Pore structure and its impact on CH4 adsorption capacity and flow capability of bituminous and subbituminous coals from Northeast China. Fuel 2013;103:258–68.
[13] Radlinski AP, Mastalerz M, Hinde AL, Hainbuchner M, Rauch H, Baron M, et al. Application of SAXS and SANS in evaluation of porosity, pore size distribution and surface area of coal. Int J Coal Geol 2004;59(3):245–71.
[14] Wang G, Shen J, Liu S, Jiang C, Qin X. Three-dimensional modeling and analysis of macro-pore structure of coal using combined X-ray CT imaging and fractal theory. Int J Rock Mech Min Sci 2019;123:104082.
[15] Tian S, Ren W, Li G, Yang R, Wang T. A theoretical analysis of pore size distribution effects on shale apparent permeability. Geofluids 2017;2017:9.
[16] Civan F. A triple-mechanism fractal model with hydraulic dispersion for gas permeation in tight reservoirs. In: SPE International Petroleum Conference and Exhibition in Mexico. Villahermosa, Mexico: Society of Petroleum Engineers; 2002. p. 9.
[17] Yang K, Lu X, Lin Y, Neimark AV. Deformation of coal induced by methane adsorption at geological conditions. Energy Fuel 2010;24(11):5955–64.
[18] Walsh JB, Brace WF. The effect of pressure on porosity and the transport properties of rock. J Geophys Res Solid Earth 1984;89(B11):9425–31.
[19] Wang K, Liu A, Zhou A. Theoretical analysis of influencing factors on resistance in the process of gas migration in coal seams. Int J Min Sci Technol 2017;27(2):315–9.
[20] Adler PM, Thovert JF. Real porous media: local geometry and macroscopic properties. Appl Mech Rev 1998;51(9):537–85.
[21] Fu X, Qin Y, Zhang W, Wei C, Zhou R. Fractal classification and natural classification of coal pore structure based on migration of coal bed methane. Chin Sci Bull 2005;50(1):66–71.
[22] Haghshenas B, Clarkson CR, Chen S. Multi-porosity multi-permeability models for shale gas reservoirs. In: SPE unconventional resources conference Canada. Calgary, Alberta, Canada: Society of Petroleum Engineers; 2013. p. 10.
[23] Han W, Zhou G, Gao D, Zhang Z, Wei Z, Wang H, et al. Experimental analysis of the pore structure and fractal characteristics of different metamorphic coal based on mercury intrusion-nitrogen adsorption porosimetry. Powder Technol 2019.
[24] Ren P, Xu H, Tang D, Li Y, Chen Z, Sun C, et al. Pore structure and fractal characterization of main coal-bearing synclines in western Guizhou, China. J Nat Gas Sci Eng 2019;63:58–69.
[25] Zhao J, Tang D, Qin Y, Xu H. Fractal characterization of pore structure for coal macrolithotypes in the Hancheng area, southeastern Ordos Basin, China. J Pet Sci Eng 2019;178:666–77.
[26] Yu B, Li J. Some fractal characters of porous media. Fractals 2001;9(3):365–72.
[27] Chen X, Yao G. An improved model for permeability estimation in low permeable porous media based on fractal geometry and modified Hagen-Poiseuille flow. Fuel 2017;210:748–57.
[28] Zheng Q, Yu B. A fractal permeability model for gas flow through dual-porosity media. J Appl Phys 2012;111(2):024316.
[29] Liu G, Liu J, Liu L, Ye D, Gao F. A fractal approach to fully-couple coal deformation and gas flow. Fuel 2019;240:219–36.
[30] Li W, Zhao H, Li S, Sun W, Wang L, Li B. A fractal model of effective stress of porous media and the analysis of influence factors. Results Phys 2018;8:920–5.
[31] Tan X-H, Li X-P, Liu J-Y, Zhang L-H, Fan Z. Study of the effects of stress sensitivity on the permeability and porosity of fractal porous media. Phys Lett A 2015;379(39):2458–65.
[32] J. Tian, J. Liu, D. Elsworth, Y.K. Leong, W. Li, J. Zeng. A dynamic fractal permeability model for heterogeneous coalbed reservoir considering multiphysics and flow regimes. Unconventional Resources Technology Conference, Denver, Colorado, 22–24 July 2019 (2019), pp. 3404–3421.
[33] Li C, Dong L, Xu X, Hu P, Tian J, Zhang Y, et al. Theoretical and experimental evaluation of effective stress-induced sorption capacity change and its influence on coal permeability. J Geophys Eng 2017;14:654.
[34] J. Zeng, J.S. Liu, W. Li, J.W. Tian, Y.K. Leong, D. Elsworth, et al. Effects of heterogeneous local swelling and multiple pore types on coal and shale permeability evolution. In: SPE Europec, Virtual (2020).
[35] Tian J, Liu J, Elsworth D, Leong YK, Li W, Zeng J. Shale gas production from reservoirs with hierarchical multiscale structural heterogeneities. J. Petrol. Sci. Eng. 2022;208. Article 109380.
[36] Ramandi HL, Mostaghimi P, Armstrong RT, Saadatfar M, Pinczewski WV. Porosity and permeability characterization of coal: a micro-computed tomography study. Int J Coal Geol 2016;154:57–68.
[37] Zhang H, Liu J, Elsworth D. How sorption-induced matrix deformation affects gas flow in coal seams: A new FE model. Int J Rock Mech Min Sci 2008;45(8):1226–36.
[38] Cui X, Bustin RM. Volumetric strain associated with methane desorption and its impact on coalbed gas production from deep coal seams. AAPG Bull 2005;89(9):1181–202.
[39] Harpalani S, Schraufnagel A. Measurement of parameters impacting methane recovery from coal seams. Int J Min Geol Eng 1990;8(4):369–84.
[40] Ziarani AS, Aguilera R. Knudsen's permeability correction for tight porous media. Transp Porous Media 2012;91(1):239–60.
[41] Klinkenberg LJ. The permeability of porous media to liquids and gases. *Drilling and production practice*. New York, New York: American Petroleum Institute; 1941:14.
[42] Ertekin T, King GA, Schwerer FC. Dynamic gas slippage: A unique dual-mechanism approach to the flow of gas in tight formations. SPE Form Eval 1986;1(01):43–52.
[43] Heid JG, McMahon JJ, Nielsen RF, Yuster ST. Study of the permeability of rocks to homogeneous fluids. *Drilling and production practice*. New York, New York: American Petroleum Institute; 1950:17.
[44] Florence FA, Rushing J, Newsham KE, Blasingame TA. Improved permeability prediction relations for low permeability sands. *Rocky mountain oil & gas technology symposium*. Denver, Colorado, U.S.A.: Society of Petroleum Engineers; 2007:18.
[45] Yao J, Sun H, Fan D-y, Wang C-c, Sun Z-x. Numerical simulation of gas transport mechanisms in tight shale gas reservoirs. Pet Sci 2013;10(4):528–37.
[46] Wang G, Ren T, Wang K, Zhou A. Improved apparent permeability models of gas flow in coal with Klinkenberg effect. Fuel 2014;128:53–61.
[47] Javadpour F. Nanopores and apparent permeability of gas flow in mudrocks (shales and siltstone). J Can Pet Technol 2009;48(08):16–21.
[48] Tang GH, Tao WQ, He YL. Gas slippage effect on microscale porous flow using the lattice Boltzmann method. Phys Rev E 2005;72(5):056301.
[49] Beskok A, Karniadakis GE. Report: a model for flows in channels, pipes, and ducts at micro and nano scales. Microscale Thermophys Eng 1999;3(1):43–77.
[50] Civan F. Effective correlation of apparent gas permeability in tight porous media. Transp Porous Media 2010;82(2):375–84.
[51] Ali Beskok GEK. Report: A model for flows in channels, pipes, and ducts at micro and nano scales. Microscale Thermophys Eng 1999;3(1):43–77.
[52] Liu J, Wang JG, Gao F, Ju Y, Tang F. Impact of micro- and macro-scale consistent flows on well performance in fractured shale gas reservoirs. J Nat Gas Sci Eng 2016;36:1239–52.
[53] Zhao Z, Ni X, Cao Y, Shi Y. Application of fractal theory to predict the coal permeability of multi-scale pores and fractures. Energy Rep 2021;7:10–8.
[54] Yin T, Liu D, Cai Y, Zhou Y, Yao Y. Size distribution and fractal characteristics of coal pores through nuclear magnetic resonance cryoporometry. Energy Fuel 2017;31(8):7746–57.
[55] Yu B, Lee LJ, Cao H. A fractal in-plane permeability model for fabrics. Polym Compos 2004;23(2):201–21.
[56] Lei G, Mo S, Dong Z, Wang CAI, Li W. Theoretical and experimental study on stress-dependency of oil–water relative permeability in fractal porous media. Fractals 2018;26(02):1840010.
[57] Tan X-H, Li X-P, Liu J-Y, Zhang L-H, Cai J. Fractal analysis of stress sensitivity of permeability in porous media. Fractals 2015;23(02):1550001.
[58] Lei G, Dong P, Wu Z, Mo S, Gai S, Zhao C, et al. A fractal model for the stress-dependent permeability and relative permeability in tight sandstones. J Can Pet Technol 2015;54(01):36–48.
[59] Si L, Li Z, Yang Y. Coal permeability evolution with the interaction between nanopore and fracture: Its application in coal mine gas drainage for Qingdong coal mine in Huaibei coalfield, China. J Nat Gas Sci Eng 2018;56:523–35.
[60] Lv Q, Chen Z, Wang M. An improved elastic-tubes model for the correlation of permeability and stress with correction for the Klinkenberg effect. J Nat Gas Sci Eng 2017;48:24–35.
[61] Wu K, Chen Z, Li X, Guo C, Wei M. A model for multiple transport mechanisms through nanopores of shale gas reservoirs with real gas effect–adsorption-mechanic coupling. Int J Heat Mass Transf 2016;93:408–26.
[62] Cao P, Liu J, Leong Y-K. General gas permeability model for porous media: bridging the gaps between conventional and unconventional natural gas reservoirs. Energy Fuel 2016;30(7):5492–505.
[63] Zhang L, Shan B, Zhao Y, Du J, Chen J, Tao X. Gas transport model in organic shale nanopores considering langmuir slip conditions and diffusion: pore confinement, real gas, and geomechanical effects. Energies 2018;11(1).
[64] Tang H, Di Y, Zhang Y, Li H. Impact of stress-dependent matrix and fracture properties on shale gas production. Energies 2017;10(7).
[65] Detournay E, Cheng AHD. Fundamentals of poroelasticity. Analysis and design methods. Elsevier; 1993. p. 113–71.
[66] Liu J, Chen Z, Elsworth D, Qu H, Chen D. Interactions of multiple processes during CBM extraction: A critical review. Int J Coal Geol 2011;87(3):175–89.
[67] Li B, Liu R, Jiang Y. A multiple fractal model for estimating permeability of dual-porosity media. J Hydrol 2016;540:659–69.
[68] Zhang Z, Xie H, Zhang R, Gao M, Ai T, Zha E. Size and spatial fractal distributions of coal fracture networks under different mining-induced stress conditions. Int J Rock Mech Min Sci 2020;132:104364.
[69] Miao T, Yu B, Duan Y, Fang Q. A fractal analysis of permeability for fractured rocks. Int J Heat Mass Transf 2015;81:75–80.
[70] Wu Y, Liu J, Elsworth D, Miao X, Mao X. Development of anisotropic permeability during coalbed methane production. J Nat Gas Sci Eng 2010;2(4):197–210.
[71] Zheng Q, Yu B, Duan Y, Fang Q. A fractal model for gas slippage factor in porous media in the slip flow regime. Chem Eng Sci 2013;87:209–15.
[72] Liu J, Chen Z, Elsworth D, Miao X, Mao X. Evaluation of stress-controlled coal swelling processes. Int J Coal Geol 2010;83(4):446–55.
[73] van Golf-Racht TD. Fundamentals of fractured reservoir engineering. Elsevier; 1982.
[74] Wei M, Liu J, Feng X, Wang C, Fang K, Zhou F, et al. Quantitative study on coal permeability evolution with consideration of shear dilation. J Nat Gas Sci Eng 2016;36:1199–207.
[75] Palmer I. Permeability changes in coal: analytical modeling. Int J Coal Geol 2009;77(1–2):119–26.
[76] Palmer I, Mansoori J. How permeability depends on stress and pore pressure in coalbeds: a new model. SPE annual technical conference and exhibition. OnePetro; 1996.

[77] Shi J-Q, Durucan S. A model for changes in coalbed permeability during primary and enhanced methane recovery. SPE Reserv Eval Eng 2005;8(04):291–9.
[78] Wang Y, Liu S, Zhao Y. Modeling of permeability for ultra-tight coal and shale matrix: a multi-mechanistic flow approach. Fuel 2018;232:60–70.
[79] Sampath K, Perera MSA, Matthai SK, Ranjith PG, Dong-yin L. Modelling of fully-coupled CO2 diffusion and adsorption-induced coal matrix swelling. Fuel 2020; 262:116486.
[80] Li Y, Tang D, Xu H, Meng Y, Li J. Experimental research on coal permeability: the roles of effective stress and gas slippage. J Nat Gas Sci Eng 2014;21:481–8.
[81] Meng Y, Li Z, Lai F. Influence of effective stress on gas slippage effect of different rank coals. Fuel 2021;285:119207.
[82] Tao Y, Liu D, Xu J, Peng S, Nie W. Investigation of the Klinkenberg effect on gas flow in coal matrices: A numerical study. J Nat Gas Sci Eng 2016;30:237–47.
[83] Zhu WC, Liu J, Sheng JC, Elsworth D. Analysis of coupled gas flow and deformation process with desorption and Klinkenberg effects in coal seams. Int J Rock Mech Min Sci 2007;44(7):971–80.